HHS Public Access

Author manuscript

Cancer Discov. Author manuscript; available in PMC 2017 October 01.

Published in final edited form as:

Cancer Discov. 2017 April ; 7(4): 391–399. doi:10.1158/2159-8290.CD-16-0611.

Adaptive Reprogramming of *De Novo* Pyrimidine Synthesis is a Metabolic Vulnerability in Triple-Negative Breast Cancer

Kristin K. Brown[1,2,3,4,5,*], **Jessica B. Spinelli**[6], **John Asara**[2,7], and **Alex Toker**[1,2,*]

[1]Department of Pathology, Beth Israel Deaconess Medical Center, Harvard Medical School, Boston 02215, Massachusetts

[2]Cancer Center, Beth Israel Deaconess Medical Center, Harvard Medical School, Boston 02215, Massachusetts

[6]Department of Cell Biology, Harvard Medical School, Boston 02115, Massachusetts

[7]Department of Medicine, Beth Israel Deaconess Medical Center, Harvard Medical School, Boston 02215, Massachusetts

Abstract

Chemotherapy resistance is a major barrier to the treatment of triple-negative breast cancer and strategies to circumvent resistance are required. Using in vitro and in vivo metabolic profiling of triple-negative breast cancer cells, we show that an increase in the abundance of pyrimidine nucleotides occurs in response to chemotherapy exposure. Mechanistically, elevation of pyrimidine nucleotides induced by chemotherapy is dependent on increased activity of the *de novo* pyrimidine synthesis pathway. Pharmacological inhibition of *de novo* pyrimidine synthesis sensitizes triple-negative breast cancer cells to genotoxic chemotherapy agents by exacerbating DNA damage. Moreover, combined treatment with doxorubicin and leflunomide, a clinically approved inhibitor of the *de novo* pyrimidine synthesis pathway, induces regression of triple-negative breast cancer xenografts. Thus, the increase in pyrimidine nucleotide levels observed following chemotherapy exposure represents a metabolic vulnerability that can be exploited to enhance the efficacy of chemotherapy for the treatment of triple-negative breast cancer.

Keywords

Metabolism; triple-negative breast cancer; chemotherapy; pyrimidine synthesis; leflunomide

[*]**Corresponding Authors:** Alex Toker, Department of Pathology and Cancer Center, Beth Israel Deaconess Medical Center, 330 Brookline Avenue, EC/CLS633A, Boston, MA 02215. Phone: 617 735 2482; Fax: 617 735 2480; atoker@bidmc.harvard.edu, Kristin K. Brown, Cancer Therapeutics Program, Peter MacCallum Cancer Centre, 305 Grattan Street, Melbourne, Victoria 3000, Australia. Phone: 613 8559 5457; Kristin.Brown@petermac.org.

[3]Present address: Cancer Therapeutics Program, Peter MacCallum Cancer Centre, Melbourne, Victoria 3000, Australia

[4]Present address: Sir Peter MacCallum Department of Oncology, The University of Melbourne, Victoria, 3010, Australia

[5]Present address: Department of Biochemistry and Molecular Biology, The University of Melbourne, Victoria 3010, Australia.

Conflict of Interest Disclosure Statement: The authors declare no conflict of interest.

Introduction

Triple-negative breast cancer (TNBC) is a molecularly heterogeneous group of diseases defined by the lack of estrogen receptor (ER), progesterone receptor (PR) and absence of human epidermal growth factor receptor-2 (HER2) amplification. Consequently, TNBCs are impervious to therapies commonly used in other breast cancer subtypes and treatment options are largely limited to conventional genotoxic chemotherapy agents including doxorubicin (Adriamycin) (1). Approximately 30% of TNBC patients achieve a pathological complete response (pCR) after chemotherapy. However, for the majority of TNBC patients with residual disease after chemotherapy, high rates of metastatic recurrence are observed and long-term prognosis is poor (2–5). Identification of novel and actionable strategies to sensitize cancer cells to chemotherapy would represent a major advance for the management of TNBC.

Cancer cells exhibit dramatic alterations in cellular metabolism, which support cell growth, proliferation and survival. Indeed, metabolic reprogramming is a recognized hallmark of cancer induced by numerous genetic or epigenetic alterations. Targeting the existing metabolic perturbations that occur in cancer cells has emerged as a promising strategy for cancer therapy (6–8). Recent studies suggest that reprogramming of cellular metabolism is also a component of the highly coordinated response to genotoxic stress (9–11). However, the metabolic response to clinically relevant genotoxic chemotherapy agents is poorly understood.

In the present study, we sought to identify adaptive metabolic reprograming events triggered upon chemotherapy exposure that can be targeted to improve the efficacy of chemotherapy for the treatment of TNBC. We show that genotoxic chemotherapy agents reprogram the *de novo* pyrimidine biosynthesis pathway to increase the production of nucleotides necessary for DNA repair. Moreover, we demonstrate that pharmacological inhibition of *de novo* pyrimidine synthesis sensitizes triple-negative breast cancer cells to clinically relevant chemotherapy agents.

Results

To examine metabolic reprogramming events that influence the cellular response to chemotherapy, we used targeted liquid chromatography-based tandem mass spectrometry (LC-MS/MS) via selected reaction monitoring to examine changes in the steady state metabolomics profile of the TNBC cell line SUM-159PT induced following an acute (10 hour) exposure to doxorubicin. Cells were treated with a concentration of doxorubicin (0.5 μM) that effectively induced DNA damage but had negligible effects on cell viability at later time points (Fig. S1A and B). Significant differences in the metabolite profiles of untreated cells and cells exposed to doxorubicin were observed (Fig. 1A). Interestingly, doxorubicin increased the abundance of the majority of pyrimidine nucleotide species, including a greater than 2-fold increase in deoxycytidine triphosphate (dCTP) and deoxythymidine triphosphate (dTTP) levels (Fig. 1B and S1C). Purine nucleotide species were also elevated in treated cells (Fig. S1D). Using a sensitive fluorescence-based assay to specifically monitor intracellular levels of nucleoside triphosphates (12), we confirmed that doxorubicin

robustly increased dCTP and dTTP levels (Fig. 1C). Elevated levels of pyrimidine nucleoside triphosphates were also observed when SUM-159PT cells were exposed to cisplatin, a platinum-based genotoxic chemotherapy agent demonstrated to induce anti-tumor responses in a subset of TNBC patients (Fig. 1C) (13). Two pathways contribute to the synthesis of pyrimidine nucleotides; nucleotides can be recycled by a salvage pathway or synthesized via the glutamine-dependent *de novo* pyrimidine synthesis pathway (Fig. 1D). Depletion of glutamine effectively eliminated the ability of doxorubicin to elevate pyrimidine nucleoside triphosphate levels (Fig. 1E), suggesting that doxorubicin modulates *de novo* pyrimidine synthesis. To determine whether the effects of doxorubicin on the steady state abundance of pyrimidine nucleotide species was due to changes in metabolic flux through the *de novo* pyrimidine synthesis pathway, we measured changes in the relative isotopic enrichment of ^{15}N-glutamine, labeled on the amide nitrogen that is incorporated into the pyrimidine ring. A significant increase in the incorporation of label into N-carbamoyl-aspartate, which is generated in the first committed step of *de novo* pyrimidine biosynthesis (Fig. 1D), was observed following doxorubicin treatment (Fig. 1F). Increased incorporation of label into dihydroorotate (DHO), orotidine-5-phosphate (OMP) and dCTP was also observed (Fig. S1E). These data reveal that reprogramming of *de novo* pyrimidine synthesis, to generate nucleotide precursors required for DNA synthesis and DNA repair, is an adaptive response to chemotherapy.

Metabolic flux through the *de novo* pyrimidine synthesis pathway is controlled by the multifunctional enzyme CAD (carbamoyl-phosphate synthetase 2, aspartate transcarbamoylase, dihydroorotase) (Fig. 1D). The carbamoyl-phosphate synthetase activity of CAD is regulated by protein kinase A (PKA)-dependent and extracellular-signal regulated kinase (ERK)-dependent phosphorylation events (14, 15). Phosphorylation of CAD by ERK relieves feedback inhibition by uridine triphosphate (UTP) and renders CAD more sensitive to activation by phosphoribosyl pyrophosphate (PRPP), thereby promoting pyrimidine synthesis. Additionally, recent studies have revealed that CAD phosphorylation by ribosomal protein S6 kinase 1 (S6K1) increases flux through the *de novo* pathway in response to growth-promoting signals (16, 17). We observed a striking increase in the phosphorylation of CAD at the ERK site (Thr456) within two hours of treating SUM-159PT cells with low-dose doxorubicin (Fig. 2A). An increase in ERK1/2 phosphorylation was also observed (Fig. 2A). By contrast, there were no measurable changes in the phosphorylation state of S6K1, or the phosphorylation state of CAD at the S6K1 site (Ser1859), in response to doxorubicin exposure (Fig. 2A). The ability of doxorubicin to increase CAD Thr456 phosphorylation was blocked by the highly selective MEK1/2 inhibitor U0126 (Fig. 2B). Interestingly, pre-treatment with U0126 also effectively suppressed the increase in pyrimidine nucleotides observed following doxorubicin exposure (Fig. 2C).

To examine the specific involvement of the *de novo* pyrimidine synthesis pathway, and more specifically CAD, to the increase in pyrimidine nucleotide levels observed following chemotherapy exposure, we pre-treated SUM-159PT cells with N-(phosphonacetyl)-l-aspartate (PALA) prior to administration of doxorubicin. PALA is a transition state analog of aspartate transcarbamoylase and potent inhibitor of CAD (18). PALA effectively abrogated the increase in dCTP levels induced by doxorubicin treatment (Fig. 2C). PALA did not inhibit doxorubicin-induced alterations in dTTP levels (Fig. 2C), consistent with previous

observations that short-term treatment with PALA does not effectively deplete dTTP pools (19). We next examined CAD Thr456 phosphorylation and pyrimidine nucleoside triphosphate levels in additional TNBC cell lines (HCC1143, MDA-MB-468, CAL51 and MDA-MB-231) and universally observed that doxorubicin stimulated CAD Thr456 phosphorylation and increased the abundance of dCTP and dTTP (Fig. 2D and E). No changes in CAD Ser1859 phosphorylation were observed (Fig. 2D). Together, these data indicate that doxorubicin mediates the posttranslational regulation of CAD activity, and moreover demonstrate that CAD is necessary for increased pyrimidine nucleoside triphosphate production in response to chemotherapy exposure.

Maintenance of an adequate pool of deoxyribonucleoside triphosphates is essential for DNA replication and DNA repair. We hypothesized that stimulation of *de novo* pyrimidine synthesis in response to chemotherapy exposure could therefore represent a metabolic vulnerability that can be exploited to circumvent chemotherapy resistance and thereby enhance the anti-tumor activity of genotoxic chemotherapy agents. Pharmacological inhibition of *de novo* pyrimidine synthesis has been examined as an anticancer strategy and multiple inhibitors of the pathway have been developed (20). We found that despite exhibiting minimal single-agent activity, PALA and two structurally distinct inhibitors (brequinar and A771726/teriflunomide) of the inner mitochondrial membrane enzyme dihydroorotate dehydrogenase (DHODH), which catalyzes the fourth step of *de novo* pyrimidine synthesis (Fig. 1D), dramatically sensitized SUM-159PT cells to doxorubicin (Fig. 3A). Moreover, we found that shRNA-mediated depletion of CAD or DHODH sensitized SUM-159PT cells to doxorubicin (Fig. S2A and B). Given that *de novo* pyrimidine biosynthesis is coupled to the mitochondrial respiratory chain via DHODH, we examined the oxygen consumption rate (OCR) of SUM-159PT cells 4 hours after doxorubicin exposure. Single agent doxorubicin had a negligible effect on the OCR and did not affect sensitivity to oligomycin and antimycin (Fig. 3B and Fig. S2C), indicating that doxorubicin does not alter mitochondrial respiration. By contrast, single agent A771726 caused a rapid decrease in OCR (Fig. S2C) that was sustained at later timepoints (Fig. 3B), further validating pharmacological inhibition of DHODH.

A771726 is the active metabolite of leflunomide, a drug used for the management of autoimmune diseases such as rheumatoid arthritis, which also exhibits some anti-tumor activity (21, 22). Given that leflunomide is widely used in the clinic, and well tolerated in humans, we examined the efficacy of a leflunomide/A771726 and chemotherapy combination. A771726 effectively blocked the increase in dCTP and dTTP levels induced by doxorubicin (Fig. 3C). Next, to confirm that the ability of A771726 to sensitize cells to chemotherapy was due to on-target inhibition of DHODH we performed a rescue experiment with uridine, which contributes to the maintenance of pyrimidine nucleotide pools via the salvage pathway. Application of exogenous uridine completely blocked the efficacy of the combination treatment confirming that A771726 sensitizes cells to chemotherapy by inhibiting *de novo* pyrimidine synthesis (Fig. 3D). Inhibition of *de novo* pyrimidine synthesis would be expected to impair the capacity of cells to repair DNA damage. Indeed, pre-treatment with A771726 exacerbated phosphorylation of the histone variant H2A.X, a marker of DNA damage, observed following doxorubicin treatment (Fig. 3E and Fig. S2D). Consistent with the notion that A771726 sensitizes cells to doxorubicin by exacerbating

DNA damage and overwhelming the DNA damage response, we observed synergy between A771726 and additional genotoxic chemotherapy agents (cisplatin, etoposide and topotecan) (Fig. 3F). By contrast, A771726 did not sensitize cells to the microtubule destabilizing chemotherapy agent paclitaxel (Fig. 3F). A771726 effectively sensitized additional TNBC cell lines (MDA-MB-231, MDA-MB-468, HCC1143, SUM-149PT, CAL-51) to doxorubicin (Fig. 3G).

Having demonstrated adaptive reprograming of *de novo* pyrimidine synthesis in vitro, we sought to examine the conservation of this response in vivo. Mice harboring MDA-MB-231 xenografts were administered doxorubicin for 24 hours. The steady-state metabolomics profile of doxorubicin-treated tumors revealed a significant increase in the abundance of multiple pyrimidine nucleotide species when compared to vehicle-treated tumors, reminiscent of the changes observed in vitro (Fig. 4A). Next, we examined the efficacy of our combination therapy strategy in vivo. Single agent leflunomide did not significantly affect the growth of MDA-MB-231 tumor xenografts in nude mice (Fig. 4B and 4C). While single agent doxorubicin administration was cytostatic, combined treatment with doxorubicin and leflunomide induced significant tumor regression (Fig. 4B and 4C). Leflunomide, doxorubicin and the combined therapy did not prevent mice from gaining weight during the course of the experiment (Fig. 4D).

Discussion

Failure to respond to conventional chemotherapy agents is a major barrier to the successful treatment of TNBC. Here, we describe adaptive metabolic reprogramming of pyrimidine synthesis as an early event that promotes chemotherapy resistance in TNBC cells in vitro and in vivo. Furthermore, we show that inhibition of the *de novo* pyrimidine synthesis pathway with leflunomide/A771726 represents a strategy to enhance the in vitro and in vivo sensitivity of TNBC cells to chemotherapy.

The metabolic pathways that contribute to nucleic acid synthesis have been targeted for cancer therapy for many decades. To this day small molecule inhibitors of these pathways, collectively referred to as antimetabolites, form a central component of therapy regimens in many cancers. As an inhibitor of the *de novo* pyrimidine synthesis pathway, leflunomide/A771726 is classified as an antimetabolite and is clinically approved for the treatment of a number of autoimmune diseases, in particular rheumatoid arthritis. However, leflunomide has also been shown to possess anti-tumor activity in a number of tumor xenograft models (22, 23). Leflunomide has been the subject of a number of clinical trials (NCT00004071, NCT00003293, NCT00001573, NCT00003775). Here, we demonstrate that when administered in combination with chemotherapy, leflunomide could be repurposed for the treatment of TNBC. Our studies support the initiation of clinical trials to examine the efficacy of combining leflunomide with genotoxic chemotherapy agents, in particular doxorubicin, for the treatment of TNBC.

TNBC tumors classified as mesenchymal stem-like (MSL) have one of the lowest response rates to anthracycline-based chemotherapy regimens (24). We show that leflunomide drastically sensitizes xenograft tumors derived from the TNBC MSL cell line MDA-MB-231

to the anthracycline doxorubicin. Moreover, our in vivo studies used a dose of doxorubicin (1 mg/kg), which is approximately 0.1 times the recommended human dose based on body surface area. This, coupled with the fact that leflunomide is well tolerated in humans, suggests that combining leflunomide with genotoxic chemotherapy agents could represent an effective strategy to treat TNBC.

The multifunctional enzyme CAD controls metabolic flux through the *de novo* pyrimidine synthesis pathway. The catalytic activities of CAD are positively influenced by ERK-dependent and S6K1-dependent phosphorylation events (14–17). In the context of chemotherapy, we find that posttranslational modification of CAD occurs exclusively at the ERK phosphorylation site (Thr456) with no observed changes in phosphorylation at the S6K1 site (Ser1859). It has been proposed that the regulation of CAD by S6K1 represents a mechanism to increase nucleotide production for RNA and DNA synthesis that accompanies cell growth. Here, we propose that the demand for nucleotides to permit DNA repair following genotoxic chemotherapy insult is instead mediated by ERK-dependent regulation of CAD activity. We demonstrate that reprogramming of *de novo* pyrimidine synthesis is a component of the highly coordinated response to genotoxic stress.

Collectively, our studies provide critical pre-clinical evidence to demonstrate that adaptive reprograming of *de novo* pyrimidine synthesis, induced in response to chemotherapy exposure, can be harnessed and exploited to improve the anti-cancer activity of genotoxic chemotherapy agents for the treatment of TNBC.

Methods

Cell culture

SUM-159PT cells were obtained from Asterand Bioscience and maintained in Ham's F12 medium (Cellgro) containing 5% fetal bovine serum (FBS; Gibco), 1 μg/mL hydrocortisone (Sigma-Aldrich) and 5 μg/mL insulin (Gibco). CAL-51 cells were a gift from K. Polyak (Dana-Farber Cancer Institute, Boston, MA, USA). All other cell lines were obtained from the American Type Culture Collection (ATCC). Cell lines were authenticated using short tandem repeat (STR) profiling no more than six months prior to experiments being performed. Cells were maintained in culture for no longer than 4 months and were routinely assayed for mycoplasma contamination. MDA-MB-231, MDA-MB-468 and CAL51 cells were maintained in DMEM (Cellgro) containing 10% FBS. Hs578t cells were cultured in DMEM containing 10% FBS and 10 μg/mL insulin. HCC1143 and HCC1806 cells were maintained in RPMI (Cellgro) containing 10% FBS. BT549 cells were cultured in RPMI media containing 10% FBS and 10 μg/mL insulin.

Chemotherapy agents and inhibitors

Doxorubicin for in vitro experiments was purchased from Cell Signaling Technology; A771726, leflunomide and doxorubicin for in vivo experiments was purchased from Selleck Chemicals; U0126, etoposide, topotecan hydrochloride, cisplatin and paclitaxel were from Tocris; brequinar was purchased from Sigma-Aldrich. N-(phosphonacetyl)-l-aspartic acid (PALA) was obtained from the Drug Synthesis and Chemistry Branch, Developmental

Therapeutics Program, Division of Cancer Treatment and Diagnosis, National Cancer Institute; Oligomycin and Antimycin A were from Sigma.

Antibodies

p-H2A.X, H2A.X, p-CAD (S1859), CAD, p-ERK (T202/Y204), ERK1/2, p-S6K (T389) and S6K antibodies were purchased from Cell Signaling Technology. P-CAD (T456) and DHODH antibodies were obtained from Santa-Cruz Biotechnology. An Alexa-Fluor 647-conjugated p-H2A.X (Ser139) antibody was purchased from BD Biosciences.

LC-MS/MS metabolomics profiling

For in vitro studies, SUM-159PT cells were maintained in full growth medium, and fresh medium was added at the time cells were treated with doxorubicin. For metabolite extraction, medium from biological triplicates was aspirated and ice-cold 80% (v/v) methanol was added. Cells and the metabolite-containing supernatants were collected and the insoluble material in lysates was pelleted by centrifugation at 10,000 *g* for 10 min. The resulting supernatant was evaporated using a refridgerated SpeedVac. For in vivo studies, ice-cold 80% (v/v) methanol was added to flash-frozen tumor tissue. Tissue was homogenized using a TissueLyser (Qiagen). The insoluble material was pelleted by centrifugation at 10,000 *g* for 10 min. The resulting supernatant was evaporated using a refridgerated SpeedVac. Samples were re-suspended using 20 μl HPLC-grade water for mass spectrometry. Ten microlitres was injected and analysed using a 5500 QTRAP hybrid triple quadrupole mass spectrometer (AB/SCIEX) coupled to a Prominence UFLC HPLC system (Shimadzu) with selected reaction monitoring (SRM). Peak areas from the total ion current for each metabolite SRM transition were integrated using MultiQuant v2.0 software (AB/SCIEX). Data analysis was performed using MetaboAnalyst.

Isotope labeling

Ham's F12 medium lacking glutamine (Sigma-Aldrich) was supplemented with 100 μM L-glutamine (amide-^{15}N). SUM-159PT cells were treated with doxorubicin for 4 hours, at which point medium containing doxorubicin was aspirated and labeled medium was added to the cells. After 1 hour of labeling, cellular metabolites were extracted as described above and quantified using SRM on a 5500 QTRAP mass spectrometer using a protocol to detect ^{15}N-labelled isotopologues of metabolites in the *de novo* pyrimidine synthesis pathway.

Deoxyribonucleoside triphosphate assay

Cells were maintained in full growth medium, and fresh medium was added at the time cells were treated with doxorubicin. In some cases, SUM-159PT cells were switched to Ham's F12 medium lacking glutamine. For metabolite extraction, medium was aspirated and ice-cold 60% (v/v) methanol was added. The insoluble material in lysates was pelleted by centrifugation at 10,000 *g* for 10 min. The resulting metabolite-containing supernatants were evaporated using a refridgerated SpeedVac. Samples were re-suspended in water and deoxyribonucleside triphosphate levels were measured as previously described (12).

Immunoblotting

Cells were washed with ice-cold PBS and lysed in radioimmunoprecipitation buffer (RIPA; 1% NP-40, 0.5% sodium deoxycholate, 0.1% SDS, 150 mmol/L NaCl, 50 mmol/L Tris-HCl, pH 7.5, protease inhibitor cocktail, 50 nmol/L calyculin A, 1 mmol/L sodium pyrophosphate, and 20 mmol/L sodium fluoride). Cell extracts were cleared by centrifugation and protein concentration was measured with the Bio-Rad DC protein assay. Lysates were then resolved on acrylamide gels by SDS-PAGE and transferred electrophoretically to nitrocellulose membrane (Bio-Rad). Blots were blocked in Tris-buffered saline (TBST) buffer (10 mmol/L Tris-HCl, pH 8, 150 mmol/L NaCl and 0.2% Tween 20) containing 5% (w/v) nonfat dry milk and then incubated with primary antibody overnight. Membranes were incubated with HRP-conjugated secondary antibody and developed using enhanced chemiluminescence substrate (EMD Millipore).

RNA-interference

For shRNA silencing of CAD and DHODH single-stranded oligonucleotides encoding CAD or DHODH target shRNA, and its complement, were synthesized: DHODH #1 sense, 5’-CCG GGT GAG AGT TCT GGG CCA TAA ACT CGA GTT TAT GGC CCA GAA CTC TCA CTT TTT G-3’; DHODH #2 antisense, 5’-AAT TCA AAA AGT GAG AGT TCT GGG CCA TAA ACT CGA GTT TAT GGC CCA GAA CTC TCA C-3’; DHODH #2 sense, 5’-CCG GCG ATG GGC TGA TTG TTA CGA ACT CGA GTT CGT AAC AAT CAG CCC ATC GTT TTT G-3’; CAD #1 sense, 5’-CCG GCG AAT CCA GAA GGA ACG ATT TCT CGA GAA ATC GTT CCT TCT GGA TTC GTT TTT G-3’; CAD #1 antisense, 5’-AAT TCA AAA ACG AAT CCA GAA GGA ACG ATT TCT CGA GAA ATC GTT CCT TCT GGA TTC G-3’; CAD #2 sense, 5’-CCG GGG GCA CAC TTA GAT ATT CCT CGA GGA ATA TCT AAG TGT GCT GCC CTT TTT G-3’; CAD #2 antisense, 5’-AAT TCA AAA AGG GCA CAC TTA GAT ATT CCT CGA GGA ATA TCT AAG TGT GCT GCC C-3’. The oligonucleotide sense and antisense pair was annealed and inserted into the pLKO.1 backbone. To produce lentiviral supernatants, HEK-293T cells were co-transfected with control or shRNA containing pLKO.1 vectors, VSVG and psPAX2 for 48 hours. Cells expressing shRNA were cultured in medium containing 2 μg/mL puromycin.

Propidium iodide viability assay

Cell viability was assayed with a prodium iodide-based plate reader assay, as previously described (25). Briefly, cells in 96-well plates were treated with a final concentration of 30 μM propidium iodide for 60 minutes at 37°C. The initial fluorescence intensity was measured before digitonin was added to each well at a final concentration of 600 μM. After incubating for 30 minutes at 37°C, the final fluorescence intensity was measured. The fraction of dead cells was calculated by dividing the background-corrected initial fluorescence intensity by the final fluorescence intensity.

Mitochondrial respiration

Mitochondrial respiration was assessed using the Seahorse XFe-96 Analyzer (Seahorse Bioscience). SUM-159PT cells (50,000 cells per well) were treated with vehicle control, 0.5 μM Doxorubicin, 20 μM A771726, or the combination (A771726 & Doxorubicin) for 4

hours in normal media conditions. Following this incubation, media was changed to a non-buffered, serum-free Seahorse Media (Seahorse Bioscience, Catalog #102353) supplemented with 5 mM glucose, 2 mM L-glutamine, and 1 mM sodium pyruvate, and the oxygen consumption rate (OCR) was measured. In addition, OCR was measured for 30 minutes upon drug treatment and cells were subsequently challenged with either 1 μM Oligomycin or 0.5 μM Antimycin A to assess their effect on mitochondrial respiration. All experiments were normalized to cell number.

Immunofluorescence

Cells plated on coverslips were fixed with 2% paraformaldehyde for 10 minutes, permeabilized with 0.5% Triton X-100, and blocked with 1% BSA in 20 mmol/L Tris-HCl, pH 7.5, for 20 minutes. Coverslips were then incubated with Alexa Fluor® 647- conjugated anti-phospho H2A.X S139 antibody (1:100) for 3 hours. After washing twice with PBS, coverslips were mounted with Prolong Gold antifade reagent containing DAPI (Life Technologies). Images of cells were acquired using a fluorescence microscope (Nikon Eclipse Ti) and digital image analysis software (NIS-Elements, Nikon).

Xenograft studies

Female nude mice (6 weeks old) were purchased from Taconic and maintained and treated under specific pathogen-free conditions. All procedures were approved by the Institutional Animal Care and Use Committee at Beth Israel Deaconess Medical Center (BIDMC) and conform to the federal guidelines for the care and maintenance of laboratory animals. The mice were injected subcutaneously with 4×10^6 MDA-MB-231 cells in medium containing 50% growth-factor-reduced, phenol red-free Matrigel (Corning). Tumor formation was examined every two to three days for the duration of the experiment. For metabolomics profiling, when tumors reached a size of 5–6 mm in diameter, mice were divided into a control group ($n = 5$ mice) and a treatment group that was exposed to 1 mg/kg doxorubicin ($n = 5$ mice). Tumors were collected and flash-frozen 24 hours after animals were exposed to vehicle or doxorubicin. For combination therapy studies, when tumors reached a size of 5–6 mm in diameter, animals were divided into a control group and treatment groups of leflunomide alone, doxorubicin alone, and leflunomide in combination with doxorubicin ($n = 5$ mice per group). Leflunomide (7.5 mg/kg) was administered on days 1–7, 10, 14, 17, 21 and 24 by i.p. injection. Doxorubicin (1 mg/kg) was administered on days 1, 7, 14 and 21 by i.p. injection. Mice were weighed on days 1, 7, 14, 21 and 28. Tumor volume was calculated using the following equation: Tumor volume = $(\pi/6)(W^2)(L)$, where W represents width, and L represents length.

Supplementary Material

Refer to Web version on PubMed Central for supplementary material.

Acknowledgments

We thank M. Yuan for technical assistance with mass spectrometry; T. Tsang and M.H. Yang for assistance with xenograft experiments; and all members of the Toker laboratory for discussions.

Financial support: This work was supported by the Ludwig Center at Harvard.

References

1. Isakoff SJ. Triple-negative breast cancer: role of specific chemotherapy agents. Cancer J. 2010; 16:53–61. [PubMed: 20164691]
2. Guarneri V, Broglio K, Kau SW, Cristofanilli M, Buzdar AU, Valero V, et al. Prognostic value of pathologic complete response after primary chemotherapy in relation to hormone receptor status and other factors. J Clin Oncol. 2006; 24:1037–1044. [PubMed: 16505422]
3. Kuerer HM, Newman LA, Smith TL, Ames FC, Hunt KK, Dhingra K, et al. Clinical course of breast cancer patients with complete pathologic primary tumor and axillary lymph node response to doxorubicin-based neoadjuvant chemotherapy. J Clin Oncol. 1999; 17:460–469. [PubMed: 10080586]
4. Liedtke C, Mazouni C, Hess KR, Andre F, Tordai A, Mejia JA, et al. Response to neoadjuvant therapy and long-term survival in patients with triple-negative breast cancer. J Clin Oncol. 2008; 26:1275–1281. [PubMed: 18250347]
5. Cortazar P, Zhang L, Untch M, Mehta K, Costantino JP, Wolmark N, et al. Pathological complete response and long-term clinical benefit in breast cancer: the CTNeoBC pooled analysis. Lancet. 2014; 384:164–172. [PubMed: 24529560]
6. Ward PS, Thompson CB. Metabolic reprogramming: a cancer hallmark even warburg did not anticipate. Cancer Cell. 2012; 21:297–308. [PubMed: 22439925]
7. Hanahan D, Weinberg RA. Hallmarks of cancer: the next generation. Cell. 2011; 144:646–674. [PubMed: 21376230]
8. Galluzzi L, Kepp O, Vander Heiden MG, Kroemer G. Metabolic targets for cancer therapy. Nat Rev Drug Discov. 2013; 12:829–846. [PubMed: 24113830]
9. Cosentino C, Grieco D, Costanzo V. ATM activates the pentose phosphate pathway promoting anti-oxidant defence and DNA repair. Embo J. 2011; 30:546–555. [PubMed: 21157431]
10. Jeong SM, Xiao C, Finley LW, Lahusen T, Souza AL, Pierce K, et al. SIRT4 has tumor-suppressive activity and regulates the cellular metabolic response to DNA damage by inhibiting mitochondrial glutamine metabolism. Cancer Cell. 2013; 23:450–463. [PubMed: 23562301]
11. Aird KM, Worth AJ, Snyder NW, Lee JV, Sivanand S, Liu Q, et al. ATM couples replication stress and metabolic reprogramming during cellular senescence. Cell Rep. 2015; 11:893–901. [PubMed: 25937285]
12. Wilson PM, Labonte MJ, Russell J, Louie S, Ghobrial AA, Ladner RD. A novel fluorescence-based assay for the rapid detection and quantification of cellular deoxyribonucleoside triphosphates. Nucleic Acids Res. 2011; 39:e112. [PubMed: 21576234]
13. Silver DP, Richardson AL, Eklund AC, Wang ZC, Szallasi Z, Li Q, et al. Efficacy of neoadjuvant Cisplatin in triple-negative breast cancer. J Clin Oncol. 2010; 28:1145–1153. [PubMed: 20100965]
14. Sigoillot FD, Evans DR, Guy HI. Growth-dependent regulation of mammalian pyrimidine biosynthesis by the protein kinase A and MAPK signaling cascades. J Biol Chem. 2002; 277:15745–15751. [PubMed: 11872754]
15. Graves LM, Guy HI, Kozlowski P, Huang M, Lazarowski E, Pope RM, et al. Regulation of carbamoyl phosphate synthetase by MAP kinase. Nature. 2000; 403:328–332. [PubMed: 10659854]
16. Ben-Sahra I, Howell JJ, Asara JM, Manning BD. Stimulation of de novo pyrimidine synthesis by growth signaling through mTOR and S6K1. Science. 2013; 339:1323–1328. [PubMed: 23429703]
17. Robitaille AM, Christen S, Shimobayashi M, Cornu M, Fava LL, Moes S, et al. Quantitative phosphoproteomics reveal mTORC1 activates de novo pyrimidine synthesis. Science. 2013; 339:1320–1323. [PubMed: 23429704]
18. Collins KD, Stark GR. Aspartate transcarbamylase. Interaction with the transition state analogue N-(phosphonacetyl)-L-aspartate. J Biol Chem. 1971; 246:6599–6605. [PubMed: 4943676]
19. Wadler S, Mao X, Bajaj R, Hallam S, Schwartz EL. N-(phosphonacetyl)-L-aspartate synergistically enhances the cytotoxicity of 5-fluorouracil/interferon-alpha-2a against human colon cancer cell lines. Mol Pharmacol. 1993; 44:1070–1076. [PubMed: 8246910]

20. Christopherson RI, Lyons SD, Wilson PK. Inhibitors of de novo nucleotide biosynthesis as drugs. Acc Chem Res. 2002; 35:961–971. [PubMed: 12437321]

21. Fragoso YD, Brooks JB. Leflunomide and teriflunomide: altering the metabolism of pyrimidines for the treatment of autoimmune diseases. Expert Rev Clin Pharmacol. 2015; 8:315–320. [PubMed: 25712857]

22. White RM, Cech J, Ratanasirintrawoot S, Lin CY, Rahl PB, Burke CJ, et al. DHODH modulates transcriptional elongation in the neural crest and melanoma. Nature. 2011; 471:518–522. [PubMed: 21430780]

23. Strawn LM, Kabbinavar F, Schwartz DP, Mann E, Shawver LK, Slamon DJ, et al. Effects of SU101 in combination with cytotoxic agents on the growth of subcutaneous tumor xenografts. Clin Cancer Res. 2000; 6:2931–2940. [PubMed: 10914743]

24. Masuda H, Baggerly KA, Wang Y, Zhang Y, Gonzalez-Angulo AM, Meric-Bernstam F, et al. Differential response to neoadjuvant chemotherapy among 7 triple-negative breast cancer molecular subtypes. Clin Cancer Res. 2013; 19:5533–5540. [PubMed: 23948975]

25. Zhang L, Mizumoto K, Sato N, Ogawa T, Kusumoto M, Niiyama H, et al. Quantitative determination of apoptotic death in cultured human pancreatic cancer cells by propidium iodide and digitonin. Cancer Lett. 1999; 142:129–137. [PubMed: 10463768]

Statement of significance

The prognosis for TNBC patients with residual disease after chemotherapy is poor. We find that chemotherapy agents induce adaptive reprogramming of *de novo* pyrimidine synthesis and show that this response can be exploited pharmacologically, using clinically approved inhibitors of *de novo* pyrimidine synthesis, to sensitize TNBC cells to chemotherapy.

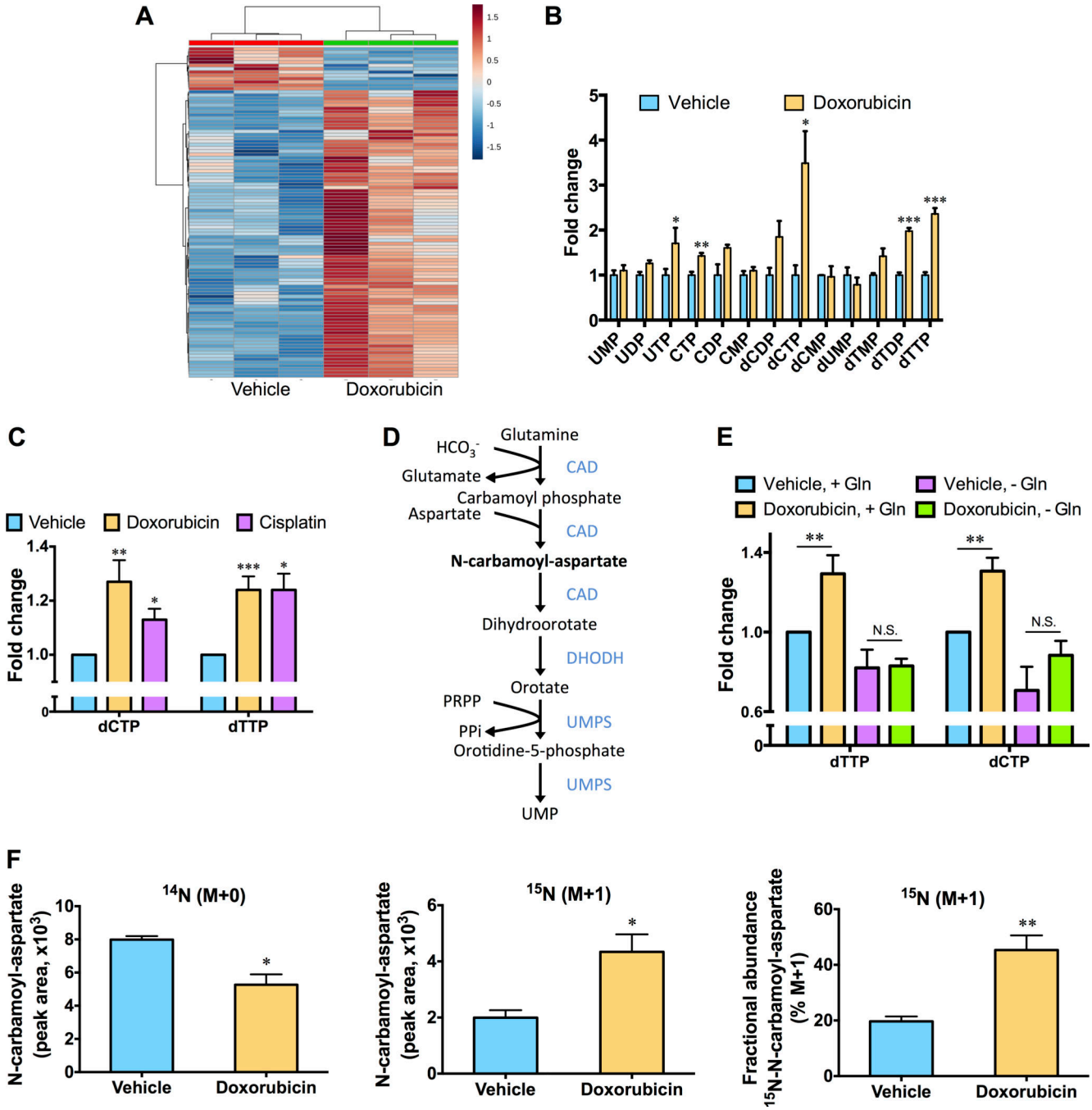

Fig. 1. Chemotherapy exposure stimulates an increase in pyrimidine nucleotides in TNBC cells

(**A**) Unbiased hierarchical clustering of relative metabolite abundances in SUM-159PT cells versus SUM-159PT cells treated with 0.5 μM doxorubicin for ten hours. (**B**) Fold changes in pyrimidine nucleotide abundances, as measured by LC-MS/MS, in vehicle treated SUM-159PT cells versus SUM-159PT cells treated with 0.5 μM doxorubicin for 10 hours. (**C**) SUM-159PT cells were treated with 0.5 μM doxorubicin or 12.5 μM cisplatin for 10 hours and pyrimidine deoxyribonucleoside triphosphate levels were monitored using a fluorescence-based assay. (**D**) Schematic of the *de novo* pyrimidine nucleotide synthesis

pathway. (**E**) Fold changes in dTTP and dCTP levels, following exposure to 0.5 μM doxorubicin for 10 hours in the absence or presence of glutamine (Gln), were monitored using a fluorescence-based assay. (**F**) Relative isotopic enrichment of L-glutamine (amide-^{15}N) into N-carbamoyl-aspartate was measured by LC-MS/MS in vehicle treated SUM-159PT cells versus SUM-159PT cells treated with 0.5 μM doxorubicin for 4 hours. All error bars represent SEM. N.S. not significant, * $P < 0.05$, ** < 0.01, *** $P < 0.001$ by a Student's *t*-test.

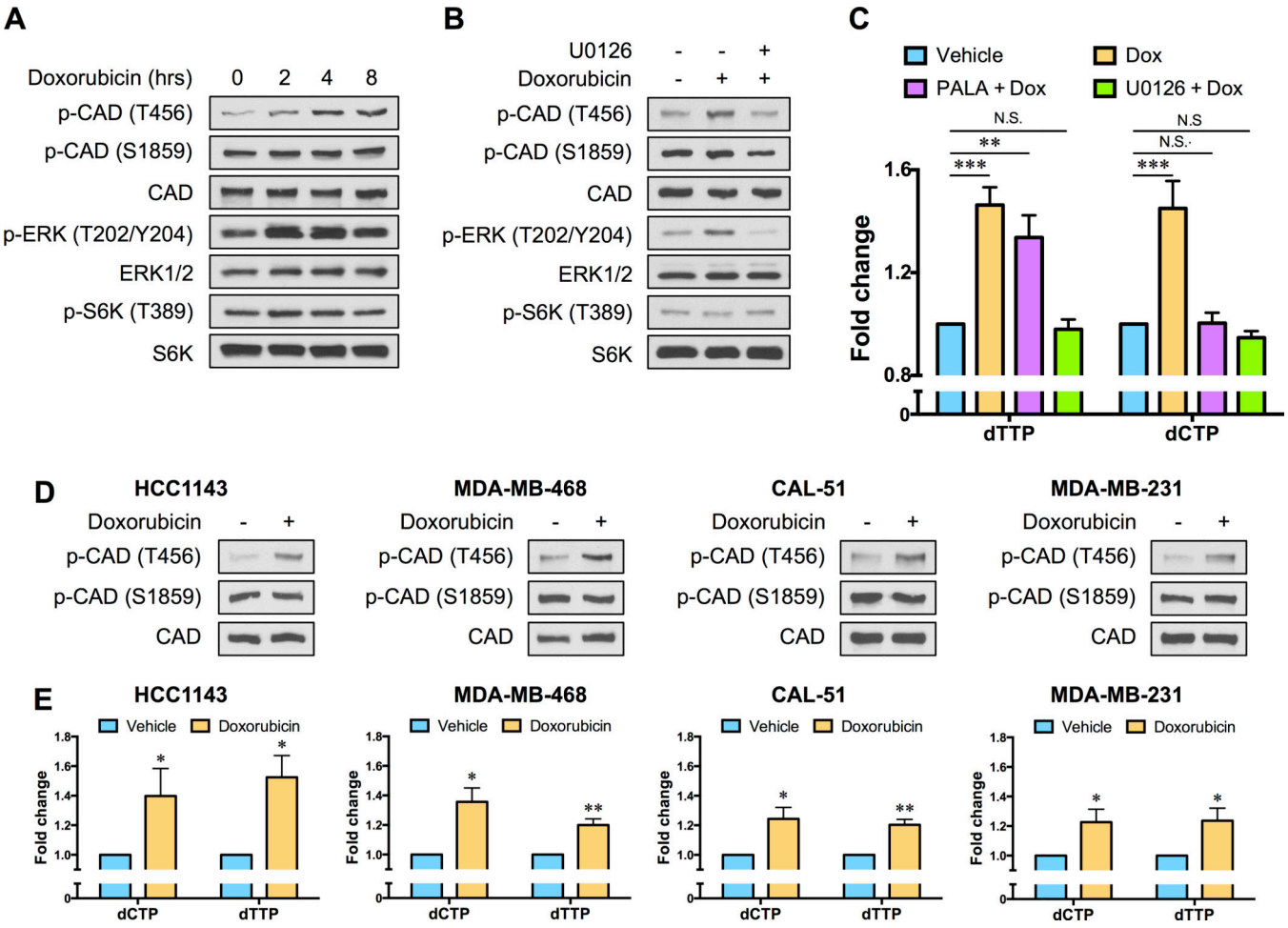

Fig. 2. Chemotherapy exposure alters the phosphorylation state of CAD to stimulate *de novo* pyrimidine nucleotide synthesis

(**A**) SUM-159PT cells were treated with 0.5 μM doxorubicin for the indicated times and the phosphorylation states of CAD, ERK and S6K1 were monitored by immunoblotting. (**B**) SUM-159PT cells were pre-treated with 5 μM U0126 for 12 hours before a 4 hour exposure to 0.5 μM doxorubicin and the phosphorylation states of CAD, ERK and S6K1 were monitored by immunoblotting. (**C**) SUM-159PT cells were treated with 0.5 μM doxorubicin for ten hours, in the absence or presence of 5 μM U0126 or 40 μM N-(phosphonacetyl)-l-aspartic acid (PALA), and pyrimidine deoxyribonucleoside triphosphate levels were monitored using a fluorescence-based assay. (**D**) TNBC cell lines (HCC1143, MDA-MB-468, CAL-51 and MDA-MB-231) were treated with 0.5 μM doxorubicin for 4 hours and changes in CAD phosphorylation were monitored by immunoblotting. (**E**) TNBC cell lines (HCC1143, MDA-MB-468, CAL51 and MDA-MB-231) were treated with 0.5 μM doxorubicin for 10 hours and pyrimidine deoxyribonucleoside triphosphate levels were monitored using a fluorescence-based assay. All error bars represent SEM. N.S. not significant, * $P < 0.05$, ** $P < 0.01$, *** $P < 0.001$ by a Student's *t*-test.

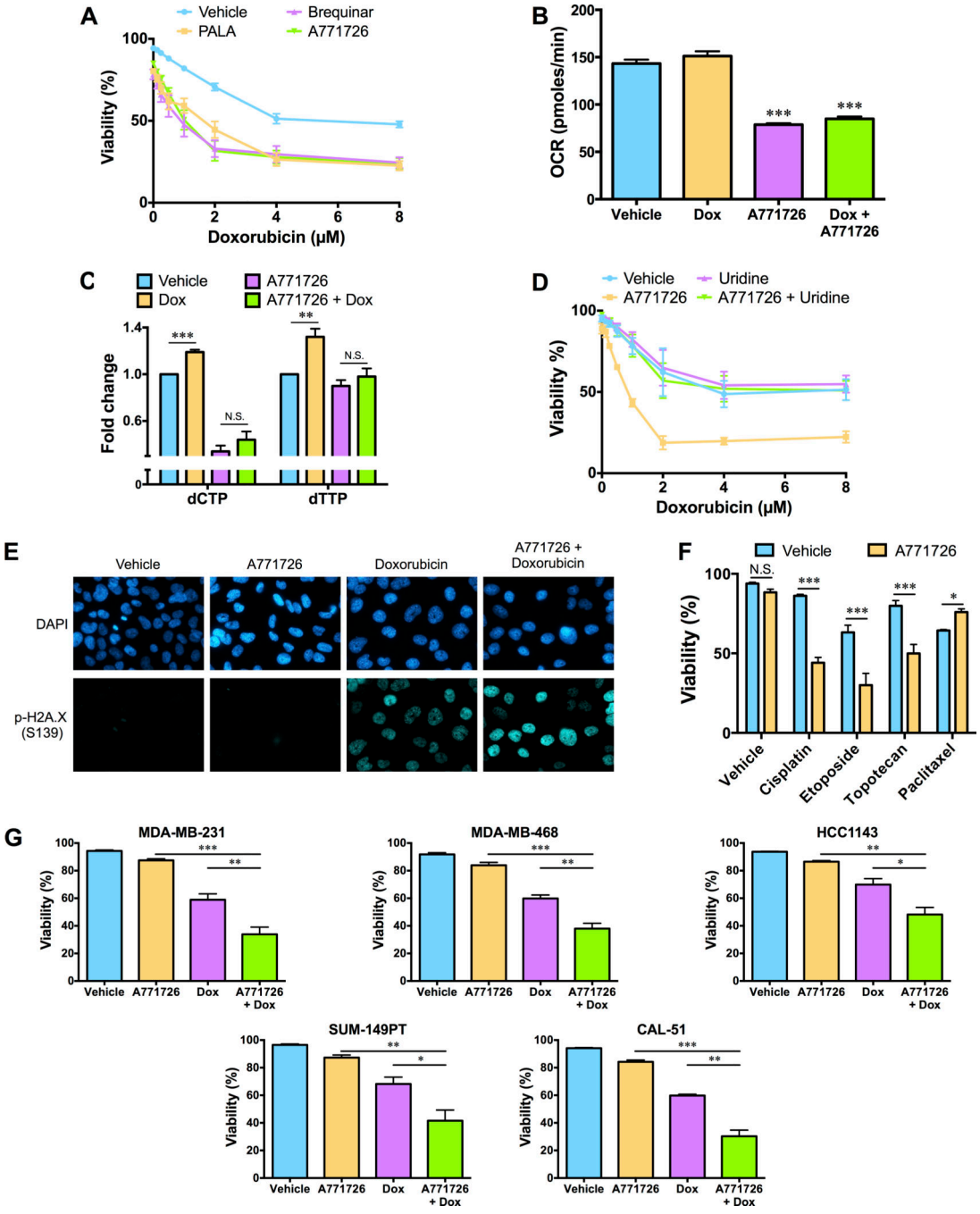

Fig. 3. Inhibition of the *de novo* pyrimidine synthesis pathway sensitizes TNBC cells to genotoxic chemotherapy

(**A**) SUM-159PT cells were pre-treated with 80 μM N-(phosphonacetyl)-l-aspartic acid (PALA), 0.3 μM brequinar or 20μM A771726 for 12 hours before exposure to doxorubicin for an additional 48 hours. The percentage of dead cells in the population was determined using a propidium iodide viability assay. (**B**) The oxygen consumption rate (OCR) of 50,000 SUM-159PT cells treated with vehicle, 0.5 μM doxorubicin (Dox), 20 μM A771726 or the combination of Dox and A771726 for 4 hours was measured using a Seahorse analyzer. (**C**)

SUM-159PT cells were pre-treated with 20μM A771726 for 12 hours before exposure to Dox for ten hours and pyrimidine deoxyribonucleoside triphosphate levels were monitored using a fluorescence-based assay. (**D**) SUM-159PT cells were pre-treated with 20 μM A771726 and 100 μM uridine for 12 hours before exposure to doxorubicin for an additional 48 hours. The percentage of dead cells in the population was determined using a propidium iodide viability assay. (**E**) SUM-159PT cells were pre-treated with 20 μM A771726 for 12 hours before exposure to doxorubicin for 10 hours. Cells were mounted on slides with DAPI after immunostaining with an Alexa-Fluor 647-conjugated p-H2A.X (Ser139) antibody. Images are representative of three independent experiments. (**F**) SUM-159PT cells were pre-treated with 20 μM A771726 for 12 hours before exposure to cisplatin (12.5 μM), etoposide (40 μM), topotecan (0.625 μM) or paclitaxel (0.5 μM) for an additional 48 hours. The percentage of dead cells in the population was determined using a propidium iodide viability assay. (**G**) TNBC cell lines (MDA-MB-231, MDA-MB-468, HCC1143, SUM-49PT, CAL-51) were pre-treated with 20 μM A771726 for 16 hours before exposure to doxorubicin for 48 hours. The percentage of dead cells in the population was determined using a propidium iodid viability assay. All error bars represent SEM. N.S. not significant, * $P < 0.05$, ** $P < 0.01$, *** $P < 0.001$ by a Student's *t*-test.

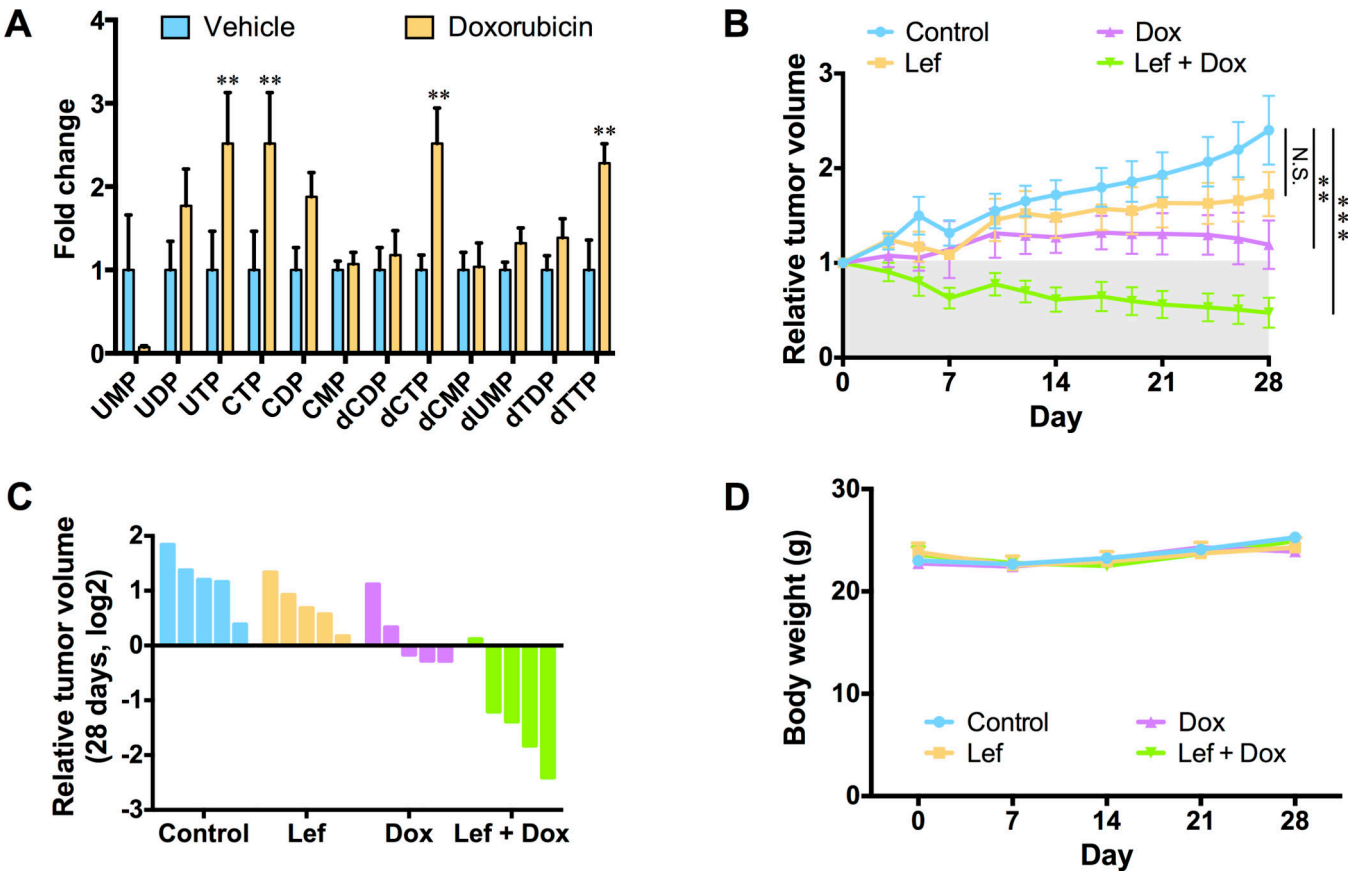

Fig. 4. Inhibition of the *de novo* pyrimidine synthesis pathway in combination with chemotherapy induces regression of TNBC tumor xenografts

(**A**) Fold changes of pyrimidine nucleotide abundances, as measured by LC-MS/MS, in vehicle treated MDA-MB-231 xenograft tumors versus MDA-MB-231 xenograft tumors treated with 1 mg/kg doxorubicin for 24 hours. (**B**) MDA-MB-231 xenografts were treated with leflunomide (Lef), doxorubicin (Dox) or a combination of leflunomide and doxorubicin (5 mice per group). Tumors were measured with calipers. (**C**) Waterfall plot depicting relative tumor volume between the treatment groups 28 days after treatment with vehicle (blue), leflunomide (orange), doxorubicin (purple) or leflunomide and doxorubicin (green). Each bar represents an individual mouse. (**D**) The body weight of mice treated with vehicle, leflunomide, doxorubicin or leflunomide and doxorubicin was monitored every 7 days for 28 days. No significant changes in body weight were observed during the course of the experiment. All error bars represent SEM. N.S. not significant, ** $P < 0.01$, *** $P < 0.001$ by a Student's *t*-test.